
THE UNIVERSITY OF MANCHESTER

School of Physics and Astronomy

MPhys Project Report

Physics with Theoretical Physics

# Topological phase transition from trivial insulator to Weyl semimetal of non-centrosymmetric 3D BiTeI crystal under pressure

*Daniil Kruklinskii*

supervised by

Dr M. Saeed BAHRAMY

January 2023

# Abstract

In this paper, the subject of the study is the topological phase transitions in inversion asymmetric bulk BiTeI crystal. It has been shown, with the aid of theoretical arguments and first-principles calculations, that under hydrostatic pressure, BiTeI undergoes a trivial insulator to Weyl semimetal transition. At a critical pressure, twelve topologically protected Weyl fermions emerge in monopole-antimonopole pairs to later annihilate and produce a band inversion. In addition, it is shown that BiTeI exhibits a strong Rashba effect, and its effects on the energy bands are analysed. It is important to study the interplay of such exotic states, as it may lead to potential theoretical discoveries and novel applications.

# Contents

# Chapter 1

# Introduction

Topological materials present a paradigm-shifting opportunity to exploit unique electronic properties that have not yet been extensively used in industry. Such properties include the emergence of new quasiparticles and unique states, effectively constituting new phases of matter. The reason that such properties are desirable is that they are robust against local perturbations because of the topological nature of the electron wave functions in those materials. Topological electrons possess a global characteristic called topological invariant. A couple of decades ago, physicists were characterizing materials based on their symmetries, commonly referred to as the Landau framework [1]; however, topological indices present a new type of analysis.

It all started with the discovery of the quantum Hall effect (QHE) by von Klitzing *et al.* [2]. Electrons in a 2D semiconductor subject to a high magnetic field seem to have a quantized Hall conductivity $\sigma_{xy}$. It was later understood by Thouless, Kohmoto, Nightingale, and den Nijs (TKNN) that this phenomenon is topological in nature [3]. It is now known that $\sigma_{xy}$ is equal to $\nu$ times $e^2/h$, where $\nu$ is a TKNN invariant that specifies the nontrivial topology of the system. TKNN invariant is a special case of another topological index called Chern number (more on that in Theory Sec. 2.3), which implies the existence of gapless edge states even without an external magnetic field [4].

Spin Hall effect (SHE) is another phenomenon which can be understood by topological considerations. This effect is essentially a double QHE with an opposite spin. Like QHE, SHE can be realized without an external magnetic field with the aid of spin-orbit coupling (SOC), as demonstrated by Kane and Mele in graphene in Ref. [5]. However, unlike QHE, SHE produces two spin currents without breaking time-reversal ($T$) symmetry, which makes materials, exhibiting this phenomenon perfect candidates for spintronic applications [6].

The breakthrough comes from the discovery of yet another topological index $Z_2$ by Kane and Mele [7]. This allowed to classify novel phases of matter, called topological insulators, according to their $Z_2$ index and demonstrated that bulk TIs exhibit previously unseen topologically-protected gapless surface states, unavailable to extensively studied 2D insulators [8,9]. As of today, many bulk TIs have been found, such as $Bi_2Se_3$, $Bi_2Te_3$ and others [10] with potential uses including dissipationless transport.

There is another unusual phase of matter, which recently got a lot of attention in condensed matter physics, called Weyl semimetal (WS). Weyl fermions, first appearing in particle physics, can be realized as quasiparticles in mate-

rials (hence the name) with inversion ($I$) symmetry or $T$-symmetry but not both [11]. These particles have intrinsic properties called chirality or chiral charge, which can be positive or negative. This property has a close connection to the Chern number [12], discussed in Sec. 2.3. Weyl fermions can only be identified in 3D crystals, where Fermi energy crosses an even number of band-touching points (BTP) formed by nondegenerate energy bands. Since the chirality of Weyl fermions is characterized by the Chern number, topologically protected surface states, called Fermi arcs, are formed [11, 12]. The existence of Weyl fermions and Fermi arcs was finally confirmed in 2015 by angle-resolved photoemission spectroscopy (ARPES) in TaAs crystals [13]. Due to the robust properties, distinct chiralities and momenta of the Weyl nodes, some Weyl semimetals exhibit unconventional superconductivity [14], making them suitable for novel technological applications.

Exotic properties of topological materials are likely to revolutionize modern technology in the next decades. Therefore, one of the main goals in solid-state physics is to be able to tune quantum materials to achieve desired properties. One of the ways is to apply an external stimulus to the crystal in the form of electric and magnetic fields or mechanical pressure. In this paper, hydrostatic pressure will be driving the topological phase transition of bulk BiTeI crystal. With theoretical and computational "first-principles" analysis, it will be shown that BiTeI undergoes a topological phase transition from a trivial insulator (TI) to a Weyl semimetal. The changes in orbital structure and spin texture of bands will be analyzed as the phase transition occurs.

# Chapter 2

# Theory

## 2.1 Structure and properties of BiTeI

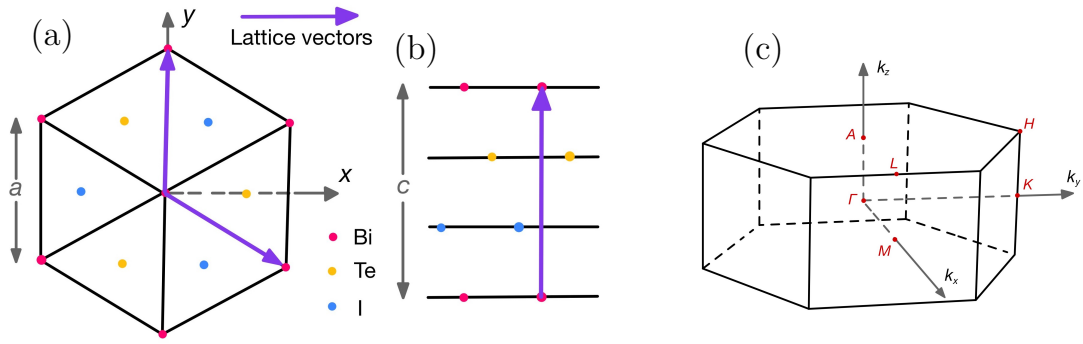


Figure 2.1: Structure of the BiTeI crystal (a) viewed in the XY-plane and (b) along the stacking z-axis. (c) The Brillouin zone of BiTeI.

BiTeI is a bulk trivially insulating crystal formed by stacking atomic layers of bismuth, tellurium, and iodine in an *A*-*B*-*C* arrangement along the $z$ direction [Fig. 2.1(b)]. In Fig. 2.1(a), it is shown that on the XY-plane, the lattice has a hexagonal structure with three atoms per unit cell (one of each element), and lattice parameters $a$ and $c$ that are measured experimentally [15] to be 4.339 Å and 6.854 Å, respectively. Since Bi and Te atoms participate in covalent bonding, forming $(BiTe)^+$ positively charged layers, and on the other hand, Bi and negatively charged $I^-$ atoms bond ionically, BiTeI crystal is polarised along the $z$ direction. Compared to bonds within BiTeI atomic layers, the full triple layers are held together by relatively weak Van der Waals forces. For this reason, as discussed in Ref. [16], despite the fact that it is still difficult to exfoliate BiTeI crystal by means of electrochemical and mechanical interventions, the liquid-phase exfoliation method is able to perform this task, which opens up new potential applications of this material.
For further theoretical discussions, it is important to consider the symmetry properties of the crystal. Since BiTeI belongs to *P3m1* space group, it lacks $I$-symmetry, which is a quintessential criterion for the Rashba effect discussed in Sec. 2.2. This material also possesses a threefold rotational symmetry ($C_{3v}$) with an axis of rotation in $z$ direction. This will also become important when discussing the WS phase of BiTeI in Sec. 4.
For first-principles calculations, the following delocalized electron orbitals are considered: six $6p$ from Bi, six $5p$ from Te, and six $5p$ from I, together

making 18 $p$-type orbitals[1]. As discussed in Ref. [17], the combined effect of negative crystal-field splitting (CFS), the result of the polar nature of BiTeI, and SOC induces a strong Rashba effect, experimentally confirmed by ARPES [18].

## 2.2 Rashba spin splitting

As originally discussed in Ref. [19], the Rashba effect is a result of the lifting of spin degeneracy of energy bands in a semiconductor. This can only occur if SOI occurs in an $I$-asymmetric material with time-reversal ($T$) symmetry (Kramers degeneracy). To understand this, consider energies of spin-opposite particles $E_\uparrow(\mathbf{k})$ and $E_\downarrow(\mathbf{k})$. If $T$-reversal symmetry holds, it implies that the particles' wave functions swap spins and directions:

$$E_\uparrow(\mathbf{k}) = E_\downarrow(-\mathbf{k}), \tag{2.1}$$

while $I$-asymmetry implies the reversal of directions of either particle:

$$E_{\uparrow/\downarrow}(\mathbf{k}) = E_{\uparrow/\downarrow}(-\mathbf{k}). \tag{2.2}$$

Hence, the combination of these operations gives the spin degeneracy

$$E_\uparrow(\mathbf{k}) = E_\downarrow(\mathbf{k}). \tag{2.3}$$

In reality, the conditions are less trivial. When considering 3D crystals, as theorised in Ref. [17], three criteria have to be fulfilled:

1. $I$-asymmetric system and strong SOC,
2. small band gap,
3. symmetrically identical bottom conduction (BCB) and top valence bands (TVB).

One can arrive at these criteria by working in the $\mathbf{k}\cdot\mathbf{p}$ perturbation theory framework. Beginning with the usual $\mathbf{k}\cdot\mathbf{p}$ Hamiltonian with SOC and applying perturbation theory (PT) to the second order, one can get

$$H_\mathbf{k} = \frac{p^2}{2m} + V + \frac{\hbar^2 k^2}{2m} + \frac{\hbar}{m}\mathbf{k}\cdot\mathbf{p} + H^{(1)} + H^{(2)} \tag{2.4}$$

with

$$H^{(1)} = \frac{\hbar^2}{4m^2c^2}(\nabla V \times \mathbf{k})\cdot\boldsymbol{\sigma} \quad \text{and} \quad H^{(2)} = \frac{\hbar}{4m^2c^2}(\Delta V \times \mathbf{p})\cdot\boldsymbol{\sigma}, \tag{2.5}$$

[1] 6 orbitals from each element comes from $p_x$, $p_y$, $p_z$ with an additional degree of freedom for the spin (two for each state).

where $\mathbf{k}$, $V$, $\mathbf{p}$, and $\boldsymbol{\sigma}$ are wavevector, crystal potential, momentum operator, and Pauli matrices, respectively, and other symbols have their usual meaning. Since the momentum of the $p$-orbital is greater than the momentum of the wave packet $H^{(2)}$ dominates the spin splitting. Then the second-order PT correction is given by

$$\Delta E_n^{(2)} = \frac{\hbar}{m} \sum_{n \neq m} \frac{\langle u_n | H^{(2)} | u_m \rangle \langle u_m | \mathbf{k} \cdot \mathbf{p} | u_n \rangle + c.c.}{E_n^{(0)} - E_m^{(0)}}, \tag{2.6}$$

where $E_n^{(0)}$ and $|u_n\rangle$ are n$^{\text{th}}$ unperturbed eigenenergies and their eigenstates. *c.c.* means complex conjugate. By looking at Eq. (2.6), one clearly sees all three criteria: 1. SOC is reflected in $H^{(2)}$, 2. energy gap $E_n^{(0)} - E_m^{(0)}$, and finally 3. $\langle u_n | H^{(2)} | u_m \rangle$, the symmetry of the eigenstates. As argued in Ref. [17], by comparing first-principles calculations of optimized and unoptimized structures of BiTeI and employing a group theory analysis of the states, it is confirmed that this material indeed satisfies all three criteria for Rashba spin-splitting (RSS), and therefore exhibits Rashba effect. Since BiTeI has $C_{3v}$ symmetry, the method of invariants can be used to show that the effective Hamiltonian in Eq. (2.4) can only be proportional to $(\sigma_x q_y - \sigma_y q_x)$, which is Rashba-type Hamiltonian.

## 2.3 Weyl fermions

The phenomenon of Weyl fermions in materials is a manifestation of topological invariants, assigned to Bloch wave function $|n(\mathbf{k})\rangle$ of electrons. In particular, these invariants are related to the Berry phase [20], which is defined as

$$\gamma_n = \int_c A_n(\mathbf{k}) \cdot d\mathbf{k}, \tag{2.7}$$

where $A_n(\mathbf{k})$ is called Berry connection and is given by

$$A_n(\mathbf{k}) = i \langle n(\mathbf{k}) | \nabla_{\mathbf{k}} | n(\mathbf{k}) \rangle. \tag{2.8}$$

$A_n(\mathbf{k})$, also called gauge field, has a corresponding Berry curvature

$$\Omega_n(\mathbf{k}) = \nabla_{\mathbf{k}} \times A_n(\mathbf{k}). \tag{2.9}$$

Since Weyl fermions behave as sources and sinks of Berry curvature, closed surface integral encompassing a Weyl fermion becomes quantized and is called Chern number or chiral charge of the Weyl node.

$$C_n = \frac{1}{2\pi} \int_s \Omega_n(\mathbf{k}) d\mathbf{S}. \tag{2.10}$$

Berry curvature is sometimes called magnetic field in **k**-space, as under $T$-reversal it transforms identically to it as follows

$$\Omega_n(\mathbf{k}) = -\Omega_{\bar{n}}(\text{-}\mathbf{k}), \tag{2.11}$$

where $|\bar{n}(\mathbf{k})\rangle$ is the $T$-reversed state of $|n(\mathbf{k})\rangle$. For that reason, Weyl fermions are sometimes called monopoles and antimonopoles. The only way for a chiral charge to change is to be created or annihilated with a partner of the opposite chiral charge [21].

## 2.4 Phase transitions in non-centrosymmetric insulators

Consider parameter space $(\alpha, k_x, k_y, k_z)$, where $\alpha$ is the external tuning parameter (pressure in this case). In general, for non-centrosymmetric gapped systems such as BiTeI, it is possible to close the gap by accidental band crossing (ABC) by choosing specific parameters in parameter space. This can be understood from codimensionality argument [21]. Since ABC occurs between two bands, topological phase transition in non-centrosymmetric systems can be analyzed by considering the corresponding effective $(2 \times 2)$ Hamiltonian

$$H = \sum_{i=1}^{3} f_i(\alpha, \mathbf{k})\sigma_i, \tag{2.12}$$

where $\sigma_{1,2,3}$ are Pauli matrices. The goal is to achieve a band touching (BT), which can only occur only if all $f_{1,2,3}(\alpha, \mathbf{k}) = 0$. The number of such $f_i(\alpha, \mathbf{k})$ is called a codimension. In this case, it is 3, and if the codimension is smaller than the number of parameters, they can be tuned to achieve BT[2]. BiTeI is a TI at ambient conditions; hence, without loss of generality, one can define a minimum $\alpha_0$, for which all $\alpha < \alpha_0$ correspond to the TI and $\alpha > \alpha_0$ gives WS (up to a certain point). The corresponding point in parameter space will be called the critical point (CP).
In general, the BT condition is satisfied for a set of parameters, forming a path in parameter space. Picking a random point on that path will not only give a gapless point but also a Weyl fermion will be present. Due to the conservation of chiral charge, pairs of monopoles and antimonopoles are created at CP and annihilated at another point, forming closed paths in $(\alpha, k_x, k_y, k_z)$.
Now it will be described how the phase transition happens. Since the gap closes at CP, all $f_i$ can be expanded to first order around $(\alpha_0, \mathbf{k}_0)$ as follows (matrix form)

[2]It is not the case for $I$-symmetric case, for which the codimension is 5

$$\mathbf{f}(\alpha, \mathbf{k}) = \Lambda \Delta \mathbf{k} + \Delta\alpha \mathbf{N}, \tag{2.13}$$

where $\Delta\mathbf{k} = \mathbf{k} - \mathbf{k}_0$, $\Lambda_{ij} = \frac{\partial f_i}{\partial k_j}$, $\Delta\alpha = \alpha - \alpha_0$ and $\mathbf{N} = \frac{\partial f_i}{\partial \alpha}$. The Jacobian $\Lambda$ has to be singular; otherwise, the BT points will exist for $\alpha < \alpha_0$, which contradicts the initial assumption. The determinant of the Jacobian is zero, which implies that there is a basis in which the eigenvalue of one basis vector is also zero. Therefore, $\Delta\mathbf{k}$ can be transformed to $\Delta\mathbf{q}$, for which Eq. (2.13) is rewritten as

$$\mathbf{f}(\alpha, \mathbf{k}) = \Delta q_2 \mathbf{u}_2 + \Delta q_3 \mathbf{u}_3 + \Delta\alpha \mathbf{N}, \tag{2.14}$$

where $\mathbf{u}_{1,2} = \Lambda \mathbf{n}_{1,2}$ and $(\mathbf{n}_1, \mathbf{n}_2, \mathbf{n}_3)$ is the new basis set.
As explained in Ref. [21], Eq. (2.14) has only trivial solutions; therefore, the term quadratic in $\Delta q_1$ has to be added. Along with the BT condition, the equation to solve is

$$(\Delta q_1)^2 \mathbf{u}_{11} + \Delta q_2 \mathbf{u}_2 + \Delta q_3 \mathbf{u}_3 + \Delta\alpha \mathbf{N} = 0. \tag{2.15}$$

The solutions are

$$\Delta q_1 \propto \sqrt{\Delta\alpha} \quad , \quad \Delta q_2 \propto \Delta\alpha \quad \text{and} \quad \Delta q_3 \propto \Delta\alpha, \tag{2.16}$$

and they ensure that $\Delta\alpha$ is always positive, which is consistent with the initial assumption. In addition, solutions in Eq. (2.16) demonstrate that the Weyl fermion pairs are created and annihilated along the $\Delta q_1$ direction.
The final consideration is the energy dispersion at the CP. By diagonalizing the Hamiltonian in Eq. (2.12), one can show that the gap is given by $E_g = 2|\mathbf{f}|$. Therefore, at CP, the energy gap disperses as

$$E_g \propto (\Delta q_1)^2 \quad , \quad \Delta q_2 \quad , \quad \Delta q_3, \tag{2.17}$$

Notice the unusual quadratic dispersion along $q_1$, the dissociation axis. Away from CP, the dispersion is linear around the monopole in all directions, as it is a relativistic particle.

# Chapter 3

# Methodology

The effect of pressure on BiTeI crystal was simulated by the VASP program [22]. The full functionality of the program is utilized to optimize the stricture of BiTeI: the LDA functional and GGA functional of Perdew-Burke-Ernzerhof (GGA-PBE). The positions of all atoms are optimized until the force becomes less than 0.005 eV Å. Two values of pressure were used, corresponding to $V/V_0 = 1$ and $V/V_0 = 0.84$, where $V_0$ is the volume of the BiTeI unit cell unaffected by external stimulus. The first value is the ambient pressure conditions, where the bulk crystal behaves as a trivial insulator. The second value is the maximally compressed state used in the analysis, which corresponds to the topological insulator behaviour of BiTeI. WIEN2K program [23] with an augmented plane wave and atomic orbitals method was used to deduce the electronic structure of BiTeI. The $R_{mt}K_{max}$ is set to 7, and $R_{mt}$ is set to 2.5 bohr for all atoms, where $R_{mt}$ and $K_{max}$ are muffin tin radii and maximum modulus of reciprocal vectors. Then for both values of pressures, using maximally localized Wannier functions and 1155-vector supercell, 18 × 18 tight-binding Hamiltonians were computed.
Hamiltonians are initially defined in the Cartesian space for each individual hopping vector (1155 in total). Discrete Fourier transform is performed to convert the 1155 Hamiltonians into one in **k**-space. For each **k**-vector, two Hamiltonians are defined: $H_{triv}$ and $H_{topo}$, corresponding to two extreme pressure conditions discussed above. The adiabatic $\alpha$ parameter is used to interpolate the two Hamiltonians to imitate the pressure changes in the lattice. Hence the total Hamiltonian is

$$H(\mathbf{k}) = (1 - \alpha)H_{triv}(\mathbf{k}) + \alpha H_{topo}(\mathbf{k}), \tag{3.1}$$

where $0 \leq \alpha \leq 1$, $\alpha = 0$ and $\alpha = 1$ correspond to $V/V_0 = 1$ and $V/V_0 = 0.84$, respectively. Henceforth, pressure/volume changes will be discussed in terms of $\alpha$.

# Chapter 4

# Results and Discussion

## 4.1 Rashba effect and orbital mixing

As discussed in Sec. 2.1 and 2.2, it is expected that BiTeI crystal possesses an interesting band structure even as the trivial insulator. As seen in Fig. 4.1(a), all 12 valence bands and six conduction bands originate as 9 $p$-type bands, but the spin degeneracy is lifted by the SOC. However, there is a special $\Gamma - A$ trajectory in the centre of the Brillouin zone (BZ) along the $k_z$ axis (see Fig. 2.1(c)). All points along this line have accidental symmetry, which preserves spin degeneracy. Since Rashba-type Hamiltonian, which couples to the spin the most (Sec. 2.2), does not have $k_z$ dependency, SOC does not lift the degeneracy. In Fig. 4.1(b) Rashba effect is clearly observed. At $k_z = \pi/c$ TVBs and BCBs are shifted from the centre of BZ by about $\pm 0.06$ Å$^{-1}$, the band gap $E_g$ between the top valence and bottom conducting bands is approximately 0.28 eV, and the so-called Rashba gap $E_R$ is 0.12 eV, which is consistent with ARPES [18]. Another strong characteristic of the Rashba effect is the opposite spins of the states, which are determined by calculating the spin expectation value of the orbital states.

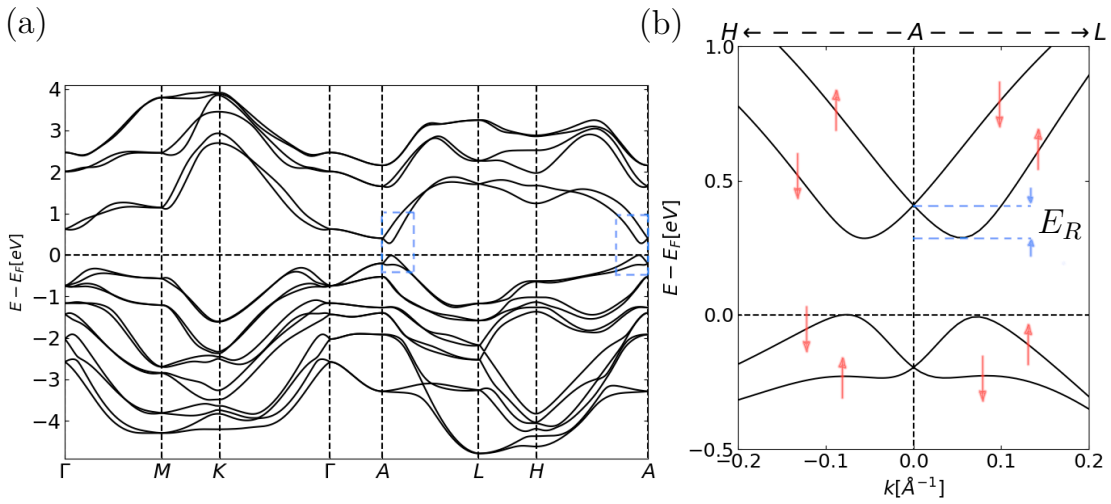


Figure 4.1: (a) shows the band structure of all 18 bands along the path of all high symmetry lines in the BZ. The Fermi level is defined at the top of the valence band. (b) is the zoomed-in band structure along *H-A-L* path. Arrows indicate the opposite spin of the states in the XY plane.

Fig. 4.3 demonstrates a topological phase transition of BiTeI. As a result of pressure change from $\alpha = 0$ to $\alpha = 0.774$ to $\alpha = 1$, the gap closes from 0.28

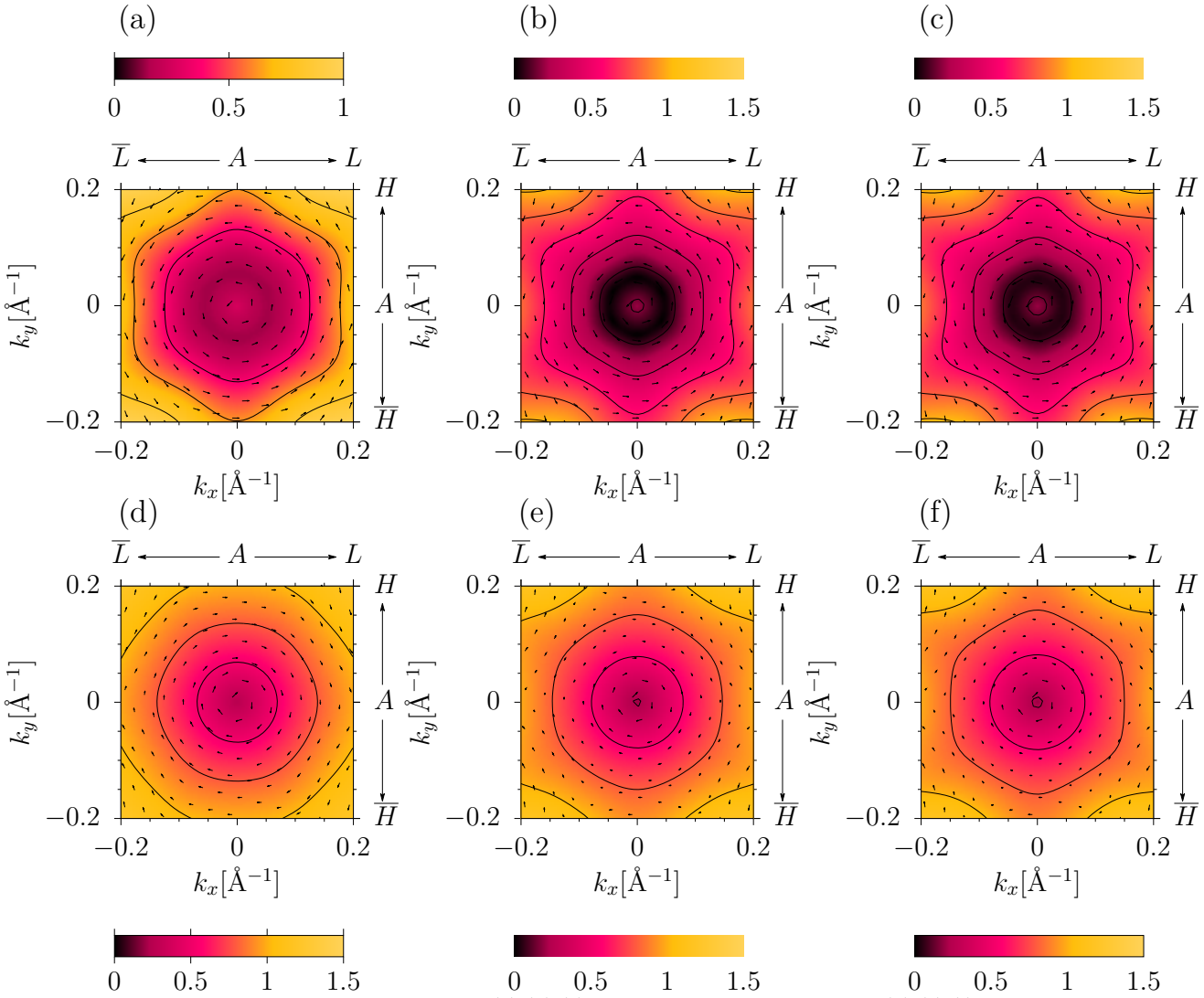


Figure 4.2: Isocontours for Rashba BCBs (a),(b),(c) and the next conduction band (d),(e),(f). Three plots for these bands are calculated for $\alpha$ =0, 0.774, 1, respectively.

eV and then reopens to $\sim 0.12$ eV. However, the orbital characteristic of the bands changes completely. At $\alpha = 0$, TVBs are dominated by $5p$-Te orbital, and BCBs are dominated by $6p$-Bi, but after the band touching point, the Bi and Te orbitals mix, producing a band inversion at $\alpha = 1$. It is interesting that after band inversion, Bi and Te orbitals are still concentrated near the band touching point, but they switch bands, compared to $\alpha = 0$. It is also important to notice that in Fig. 4.3(b), energy dispersion becomes linear around the BT point, which signals the formation of Dirac fermions. It will be shown that these are actually Weyl fermions.

The isocontours in Fig. 4.2 reflect the spin textures of the BCBs of the Rashba splitting (top) and the next conduction band (bottom). As seen from the plots, the spin textures of the bands have different helicities. Obviously, for BCBs at $\alpha > 0.774$, as already known, the gapless state emerges, but there is also unusual warping of the isocontours.

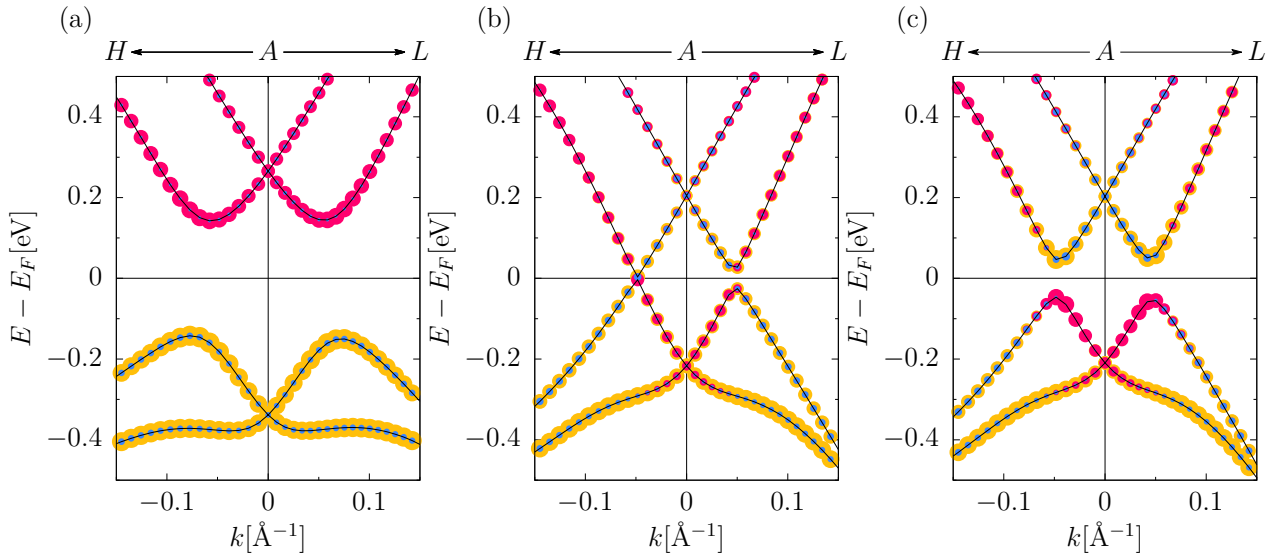


Figure 4.3: Band structure of TVBs and BCBs along $H - A - L$ line for (a) $\alpha = 0$, (b) $\alpha = 0.774$ and (c) $\alpha = 1$. Yellow, magenta and blue colouring indicate the presence of $5p$-Te, $6p$-Bi and $5p$-I states, respectively.

## 4.2 Weyl semimetal

BiTeI enters a Weyl semimetal state for $0.774 < \alpha < 0.796$. In Fig. 4.4(a), continuous Weyl trajectories are shown, as predicted in Sec. 2.4. Pairs of Weyl fermions emerge at $\alpha = 0.774$ at the creation points and migrate along the trajectories as $\alpha$ increases until they meet again at the annihilation points when $\alpha = 0.796$. It is crucial that these quasiparticles, due to the conservation of chiral charge, are created at the same point with opposite chiralities. The sum chiral charges of the pair must always add to zero. When Weyl fermions annihilate, they do so with a chirally opposite partner.

Fig. 4.4(b) shows the dispersion of energies for three orthogonal paths that, marked in Fig. 4.4(a). As predicted by the theory for non-centrosymmetric materials, these dispersions indeed obey Eq.(2.17). The tangential path (red) is quadratic at the annihilation point, while the two others are linear. The same behaviours are tested at the creation point, and it is confirmed that when $\alpha = 0.774$, there are a quadratic tangential and two linear normal paths. On the other hand, different behaviour is observed on any other point of the trajectory. When an isolated Weyl fermion travels along the trajectory, it possesses a linear dispersion in all directions, including the tangential. It is because the dispersion behaves essentially like for the Dirac fermion or other relativistic particles.

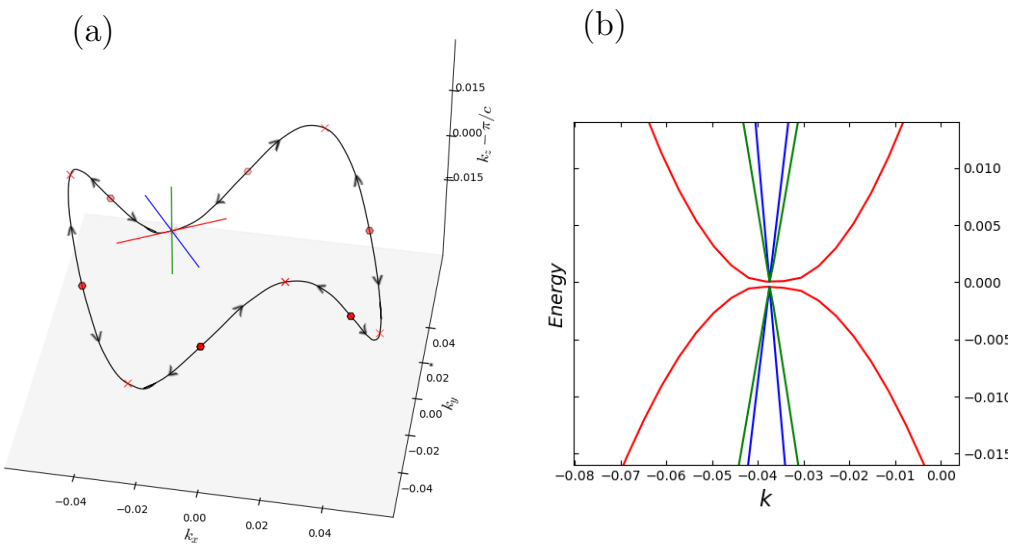


Figure 4.4: (a) shows trajectories of Weyl nodes in 3D. Arrows indicate the directions of motion of the nodes as $\alpha$ is increased. Red circles show creation points, and red crosses show annihilation points. (b) Energy dispersion along the three orthogonal directions at the annihilation point.

Let's consider the symmetries of the BiTeI Weyl semimetallic state. A view from above (Fig. 4.5(a)), the symmetry becomes apparent. Due to the $C_{3v}$ rotational symmetry, when computing the path of Weyl fermions, one is only required to analyse one-third of the azimuthal angle $\theta$, the symmetry rules out the rest. If one draws a line from the centre of the BZ and rotates it with $k_z$ being the axis of rotation from zero to $\theta$ degrees and records it, the same video would be recorded if the rotation started at $2\pi/3$. Also, mirror

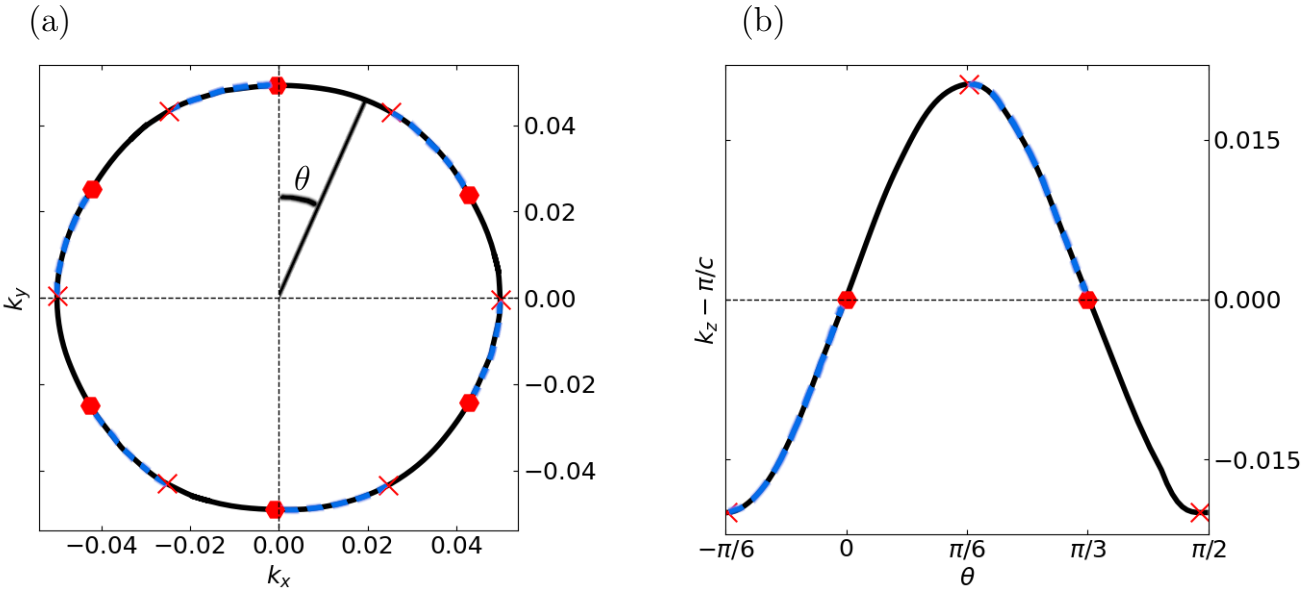


Figure 4.5: Trajectories of Weyl nodes projected on (a) the ($k_x$, $k_y$) plane and (b) viewed along the $k_z$ direction from the (0,0,$k_z - \pi/c$) on the BZ. Blue and black lines indicate the trajectories of monopoles and antimonopoles.

operation would reverse the chiral charge of the fermions. One might think that Weyl nodes are sixfold symmetric, but that is incorrect, and the reason is easily seen by looking at the vertical plane of the Weyl trajectory in Fig. 4.5. Combining all these thoughts, for $\alpha = 0.774$ twelve, Weyl fermions emerge at six creation points on the $k_z = \pi/c$ plane. For $0.774 < \alpha < 0.796$, the pair travels way from each other, one up and the other down along the trajectory. Then at $\alpha = 0.796$, the Weyl fermion from one pair annihilates with an oppositely charged fermion from another pair at six annihilation points. No path is broken, and the chiral charge is conserved.

# Chapter 5

# Conclusion

To summarise, it is shown with first-principles calculations that bulk BiTeI crystal indeed undergoes a topological phase transition from trivial insulator to Weyl semimetal, agreeing with the theoretical arguments based on the Hamiltonian for non-centrosymmetric systems. Twelve Weyl nodes are shown to emerge as a result of applying hydrostatic pressure. Moreover, they are created and annihilated in pairs of opposite chirality, in agreement with the conservation of chiral charge, which is topological in nature and related to the Chern number. Furthermore, BiTeI, satisfying theoretical conditions for Rashba spin splitting, indeed exhibits a strong Rashba effect with $E_R \sim 0.12$ eV and $E_g \sim 0.28$ eV. For $0.774 < \alpha < 0.796$, BiTeI is Weyl semimetal, but for $\alpha > 0.796$ another gapped state emerges, possessing a band inversion.
BiTeI proved to be a material that is very rich for novel quantum and topological phenomena. The interplay between such unique states may lead to further theoretical discoveries. As a Rashba semiconductor, it can be used in spintronics [6], as a Weyl semimetal, it has the potential for exotic superconductor applications [14] and possibly many more.

# Bibliography


[1] L. D. Landau, "On the theory of phase transitions," *Zh. Eksp. Teor. Fiz.*, vol. 7, pp. 19–32, 1937.

[2] K. v. Klitzing, G. Dorda, and M. Pepper, "New method for high-accuracy determination of the fine-structure constant based on quantized hall resistance," *Phys. Rev. Lett.*, vol. 45, pp. 494–497, Aug 1980. [Online]. Available: https://link.aps.org/doi/10.1103/PhysRevLett.45.494

[3] D. J. Thouless, M. Kohmoto, M. P. Nightingale, and M. den Nijs, "Quantized hall conductance in a two-dimensional periodic potential," *Phys. Rev. Lett.*, vol. 49, pp. 405–408, Aug 1982. [Online]. Available: https://link.aps.org/doi/10.1103/PhysRevLett.49.405

[4] F. D. M. Haldane, "Model for a quantum hall effect without landau levels: Condensed-matter realization of the "parity anomaly"," *Phys. Rev. Lett.*, vol. 61, pp. 2015–2018, Oct 1988. [Online]. Available: https://link.aps.org/doi/10.1103/PhysRevLett.61.2015

[5] C. L. Kane and E. J. Mele, "Quantum spin hall effect in graphene," *Phys. Rev. Lett.*, vol. 95, p. 226801, Nov 2005. [Online]. Available: https://link.aps.org/doi/10.1103/PhysRevLett.95.226801

[6] S. Murakami, N. Nagaosa, and S.-C. Zhang, "Dissipationless quantum spin current at room temperature," *Science*, vol. 301, no. 5638, pp. 1348–1351, 2003. [Online]. Available: https://www.science.org/doi/abs/10.1126/science.1087128

[7] C. L. Kane and E. J. Mele, "$Z_2$ topological order and the quantum spin hall effect," *Phys. Rev. Lett.*, vol. 95, p. 146802, Sep 2005. [Online]. Available: https://link.aps.org/doi/10.1103/PhysRevLett.95.146802

[8] L. Fu, C. L. Kane, and E. J. Mele, "Topological insulators in three dimensions," *Phys. Rev. Lett.*, vol. 98, p. 106803, Mar 2007. [Online]. Available: https://link.aps.org/doi/10.1103/PhysRevLett.98.106803

[9] M. Z. Hasan and C. L. Kane, "Colloquium: Topological insulators," *Rev. Mod. Phys.*, vol. 82, pp. 3045–3067, Nov 2010. [Online]. Available: https://link.aps.org/doi/10.1103/RevModPhys.82.3045

[10] H. Zhang, C. Liu, X. liang Qi, X. Dai, Z. Fang, and S.-C. Zhang, "Topological insulators in bi2se3, bi2te3 and sb2te3 with a single dirac cone on the surface," *Nature Physics*, vol. 5, pp. 438–442, 2009.

[11] X. Wan, A. M. Turner, A. Vishwanath, and S. Y. Savrasov, "Topological semimetal and fermi-arc surface states in the electronic structure of

pyrochlore iridates," *Phys. Rev. B*, vol. 83, p. 205101, May 2011. [Online]. Available: https://link.aps.org/doi/10.1103/PhysRevB.83.205101

[12] M. Z. Hasan, S.-Y. Xu, and G. Bian, "Topological insulators, topological superconductors and weyl fermion semimetals: discoveries, perspectives and outlooks," *Physica Scripta*, vol. 2015, 12 2015.

[13] S.-Y. Xu, I. Belopolski, N. Alidoust, M. Neupane, G. Bian, C. Zhang, R. Sankar, G. Chang, Z. Yuan, C.-C. Lee, S.-M. Huang, H. Zheng, J. Ma, D. Sanchez, B. Wang, A. Bansil, F. Chou, P. Shibayev, H. Lin, and M. Z. Hasan, "Discovery of a weyl fermion semimetal and topological fermi arcs," *Science (New York, N.Y.)*, vol. 349, 07 2015.

[14] T. Meng and L. Balents, "Weyl superconductors," *Phys. Rev. B*, vol. 86, p. 054504, Aug 2012. [Online]. Available: https://link.aps.org/doi/10.1103/PhysRevB.86.054504

[15] A. V. Shevelkov, E. V. Dikarev, R. V. Shpanchenko, and B. A. Popovkin, "Crystal structures of bismuth tellurohalides bitex (x = cl, br, i) from x-ray powder diffraction data," *Journal of Solid State Chemistry*, vol. 114, pp. 379–384, February 1995.

[16] G. Bianca, C. Trovatello, A. Zilli, M. I. Zappia, S. Bellani, N. Curreli, I. Conticello, J. Buha, M. Piccinni, M. Ghini, M. Celebrano, M. Finazzi, I. Kriegel, N. Antonatos, Z. Sofer, and F. Bonaccorso, "Liquid-phase exfoliation of bismuth telluride iodide (bitei): Structural and optical properties of single-/few-layer flakes," *ACS Applied Materials & Interfaces*, vol. 14, no. 30, pp. 34 963–34 974, 2022, pMID: 35876692. [Online]. Available: https://doi.org/10.1021/acsami.2c07704

[17] M. S. Bahramy, R. Arita, and N. Nagaosa, "Origin of giant bulk rashba splitting: Application to bitei," *Phys. Rev. B*, vol. 84, p. 041202, Jul 2011. [Online]. Available: https://link.aps.org/doi/10.1103/PhysRevB.84.041202

[18] K. Ishizaka, M. S. Bahramy, H. Murakawa, M. Sakano, T. Shimojima, T. Sonobe, K. Koizumi, S. Shin, H. Miyahara, A. Kimura, K. Miyamoto, T. Okuda, H. Namatame, M. Taniguchi, R. Arita, N. Nagaosa, K. Kobayashi, Y. Murakami, R. Kumai, and Y. Tokura, "Giant rashba-type spin splitting in bulk bitei," *Nature materials*, vol. 10, pp. 521–6, 06 2011.

[19] E. I. Rashba, "Properties of semiconductors with an extremum loop. 1. cyclotron and combinational resonance in a magnetic field perpendicular to the plane of the loop," *Sov. Phys. Solid State*, vol. 2, pp. 1109—1122, 1960.

[20] D. Xiao, M.-C. Chang, and Q. Niu, "Berry phase effects on electronic properties," *Rev. Mod. Phys.*, vol. 82, pp. 1959–2007, Jul 2010. [Online]. Available: https://link.aps.org/doi/10.1103/RevModPhys.82.1959

[21] S. Murakami and S.-i. Kuga, "Universal phase diagrams for the quantum spin hall systems," *Phys. Rev. B*, vol. 78, p. 165313, Oct 2008. [Online]. Available: https://link.aps.org/doi/10.1103/PhysRevB.78.165313

[22] G. Kresse and et al., "Vienna ab initio software packages (vasp) version 5.2.8," 2010. [Online]. Available: http://cms.mpi.univie.ac.at/vasp/

[23] P. Blaha and et al, "Wien2k package, version 10.1," 2010. [Online]. Available: http://www.wien2k.at